American Mineralogist, Volume 95, pages 563–573, 2010

Thermo-chemical and thermo-physical properties of the high-pressure phase anhydrous B ($Mg_{14}Si_5O_{24}$): An ab-initio all-electron investigation

G. Ottonello,[1,*] B. Civalleri,[2] J. Ganguly,[3] W.F. Perger,[4] D. Belmonte,[1] and M. Vetuschi Zuccolini[1]

[1]Laboratorio di Geochimica at DIPTERIS, Università di Genova, Corso Europa 26, 16132 Genova, Italy
[2]Dipartimento di Chimica IFM and NIS Centre of Excellence, Università di Torino, Via Giuria 7, 10125 Torino, Italy
[3]Department of Geosciences, University of Arizona, Tucson, Arizona 85721, U.S.A.
[4]Department of Physics, Michigan Technological University, 1400 Townsend Drive, Houghton, Michigan 49931-1295, U.S.A.

Abstract

Using the hybrid B3LYP density functional method, we computed the ab-initio thermo-chemical and -physical properties of the mineral anhydrous B (Anh-B), which has been recently suggested as a potential phase responsible for the X-discontinuity in the Earth's mantle at ~300 km depth through the reaction forsterite + periclase = Anh-B, and also to likely split the 410 km discontinuity within the interior of a cold slab through the reaction wadsleyite/ringwoodite = Anh-B + stishovite. We first conducted an investigation of the static properties through a symmetry-preserving relaxation procedure and then computed, on the equilibrium structure, harmonic vibrational modes at the long-wavelength limit corresponding to the center of the Brillouin zone ($\mathbf{k} \rightarrow 0$). While optic modes are the eigenvectors of the Hessian matrix at Γ point, acoustic modes were obtained by solving the non-zero components of the strain matrix. Following the Kieffer model, acoustic branches were assumed to follow sine wave dispersion when traveling within the Brillouin zone. All thermodynamic properties that depend on vibrational frequencies namely, heat capacities, thermal expansion, thermal derivative of the bulk modulus, thermal correction to internal energy, enthalpy, Gibbs free energy, thermal pressure and Debye temperature, were computed on the basis of quasi-harmonic mode-gamma analysis of the volume effects on vibrational frequencies. Moreover, the strain tensor was used to calculate several thermo-physical properties of geophysical interest (transverse and longitudinal wave velocities, shear modulus, Young's modulus, and Poisson's ratio). The ab-initio results derived in this study and the available data on molar volumes were used to calculate the univariant equilibrium forsterite + periclase = Anh-B. The results are in satisfactory agreement with the reversed experimental data of Ganguly and Frost (2006).

Keywords: Anhydrous B, thermodynamic properties, ab-initio, density functional theory, X-discontinuity, subduction

Introduction

Recent improvements in computational capability, including the development of accurate quantum chemical computational codes, have made the calculation of the properties of mantle minerals at high *P-T* conditions a realistic goal (Stixrude et al. 1999; Oganov et al. 2002, 2005; Ottonello et al. 2009a, 2009b). Though quite demanding, the computational approach offers an independent way of assessing the various thermo-chemical and -physical parameters that are necessary to constrain the stability limits of the mantle minerals and the mineralogically dependent rheology of the mantle. The ab-initio results could help fill important gaps in our database for minerals and also provide independent checks on the thermo-chemical and thermo-physical data that were determined experimentally or retrieved from experimental phase equilibria and calorimetric data in the internally consistent databases. It is hoped that, in conjunction with direct experimental measurements of mineral properties and stabilities, the ab-initio results would ultimately contribute significantly to the development of reliable internally consistent and accurate databases for the investigation of mantle properties and processes (also see Cygan and Kubicki 2001). Ganguly and Frost (2006) recently determined the equilibrium boundary of the reaction

forsterite (Fo) + periclase (Per) = anhydrous phase B (Anh-B) (A)

at 900–1600 °C by reversed experiments in a multi-anvil apparatus, and used the retrieved Gibbs free energy of formation of Anh-B to calculate the stability field of Anh-B + stishovite (Stv) with respect to wadsleyite (β-olivine-Wds) and ringwoodite (γ-olivine-Rwd). They suggested that reaction A could be responsible for the so-called X-discontinuity in the mantle that, although sporadic, is found at ~260–330 km depth in a range of mantle environments from seismic studies (Revenaugh and Jordan 1991; Williams and Revenaugh 2005; Bagley and Revenaugh

* E-mail: giotto@dipteris.unige.it

2008). Polymorphic mineralogical transformations, namely the orthorhombic to monoclinic transformation of ferromagnesian pyroxenes (Woodland 1998) and coesite to stishovite transformation within MORB-derived mantle eclogites (Williams and Revenaugh 2005) have also been suggested as possible explanations for the X-discontinuity. Revenaugh and co-workers (op. cit.) have discounted the orthorhombic to monoclinc transition of pyroxene as a potential candidate for the 300 km discontinuity based on seismological grounds. However, the argument of Bagley and Revenaugh (2008) against the suggestion of Ganguly and Frost (2006) is completely flawed as they misinterpreted the phase diagram and concluded that the reaction Fo + Per = Anh-B could only be accessed by a subduction zone geotherm and hence is not a viable reaction for the explanation of the X-discontinuity, while on the contrary a normal mantle adiabat crosses the reaction boundary.

The reaction:

$$\text{Anh-B} + \text{Stv} = \text{Wds/Rwd} \quad \text{(B)}$$

as calculated by Ganguly and Frost (2006) could, however, only be accessed by the *P-T* trajectory that develops within a cold subducting slab such as Tonga. If this reaction indeed has the topology and *P-T* location suggested by these workers, then there may be an "eye-shaped" splitting of the 410 km discontinuity within the interior of a sufficiently cold slab as a result of the breakdown of Wds/Rwd to Anh-B + Stv at low temperature. However, the suggested *P-T* locations of the bounding reactions defining the stability field of Anh-B are at too low temperatures to be amenable for experimental determination in a multi-anvil apparatus within reasonable laboratory time scales.

The main purpose of the present research is to calculate, as part of our continued project on the ab-initio calculations of the properties of mantle minerals (Ottonello et al. 2009a, 2009b), the thermodynamic properties of Anh-B, using the same approach that we adopted earlier, and then use the data to calculate phase equilibria of the mineral at high *P-T* conditions. As in our previous works, all calculations were carried out at the DFT/B3LYP level of theory by means of a developmental version of the CRYSTAL code (Dovesi et al. 2006). The computational details of the procedure adopted to compute the structural, vibrational, and elastic properties of Anh-B at the athermal limit are reported in Appendix 1[1]. The evaluation of the seismic properties will be presented in a separate paper that addresses the general issue of the X-discontinuity from both seismological and geological perspectives. However, because the knowledge of acoustic modes is essential for the evaluation of the thermophysical properties, we show here in some detail how these were addressed by building the strain tensor of Anh-B and solving the Kelvin-Christoffel determinant. We demonstrate the reliability of the calculated thermodynamic properties of Anh-B through comparison of the calculated equilibrium boundary for the reaction Fo + Per = Anh-B with the experimental data of Ganguly and Frost (2006). Self-consistent calculation of reaction B requires some refinement of the ab-initio thermochemical data for the Mg_2SiO_4 polymorphs and stishovite (Ottonello et al. 2009a, 2009b). This problem will be addressed in a later publication.

[1] Deposit item AM-10-015, Appendix 1. Deposit items are available two ways: For a paper copy contact the Business Office of the Mineralogical Society of America (see inside front cover of recent issue) for price information. For an electronic copy visit the MSA web site at http://www.minsocam.org, go to the *American Mineralogist* Contents, find the table of contents for the specific volume/issue wanted, and then click on the deposit link there.

Static calculations

The mineral anhydrous B, $Mg_{14}Si_5O_{24}$, crystallizes in the orthorhombic system (crystal class Orthorhombic Bipyramidal, space group *Pmcb*). There are 86 atoms in the unit cell ($Z = 2$), and 18 irreducible atoms in the conventional cell, most of which are located in the general positions.

Cell optimization was carried out with a symmetry-preserving relaxation procedure (SPR) by exploring, at selected values of V, the minimum energy a/b and c/b ratios and internal coordinates. The molar volume at the athermal limit was obtained by exploiting the full optimization procedure of the code (Dovesi et al. 2006; see also Appendix 1[1]).

The agreement between the calculated and the experimental values of cell edges (Critchon et al. 1999; Finger et al. 1991) is satisfactory (–0.0003 for the a/b ratio and +0.0005 for the c/b ratio at the static limit and $P = 0$ GPa) although the B3LYP volume is 2.4–2.8% higher than that determined experimentally (Fig. 1; Table 1).

The SPR static potential well (Fig. 2) was utilized to investigate the compressibility of the substance at 0 K and its thermal expansion at higher T through quasi-harmonic procedures.

Fitting the potential well calculated at B3LYP level with the Birch-Murnaghan (BM) third-order EoS yields a static bulk modulus $K_0 = 155.00$ GPa and a pressure derivative $K' = 4.140$. These values are, respectively, somewhat higher and lower than those experimental values reported by Crichton et al. (1999) ($K_0 = 151.5 \pm 0.9$ GPa, $K' = 5.5 \pm 0.3$) but substantially consistent with the value of K_0 obtained from the elastic constants (see below).

Vibrational calculations

Optic mode. The Born-Oppenheimer potential energy surface of a system with n nuclei, $V(\mathbf{x})$, is a function of vector $\mathbf{x}$ of the $3N$ coordinates of the atoms in a system. In the harmonic approximation, it takes the form:

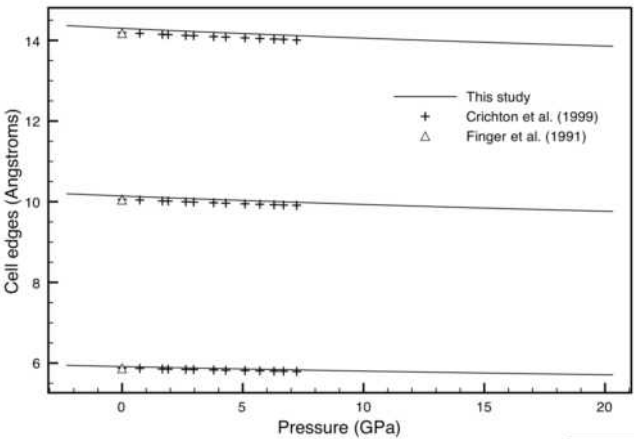

FIGURE 1. Computed a, b, and c cell edges vs. pressure. Experimental data are plotted for comparison.

TABLE 1. Cell volume and cell edges of Anh-B under various compressional states

V (Å³)	*a* (Å)	*b* (Å)	*c* (Å)	*a*/*b*	*c*/*b*	Ref.	*P* (GPa)
870.719	5.9435	14.3649	10.1983	0.4138	0.7099	1	−2.285
838.810	5.8745	14.1937	10.0592	0.4139	0.7087	2	0.000
838.804	*5.8747*	*14.1941*	*10.0591*	*0.4139*	*0.7087*	*2*	*0.000*
857.574	*5.9135*	*14.2992*	*10.1418*	*0.4136*	*0.7093*	*1*	*0.000*
856.101	5.9101	14.2917	10.1355	0.4135	0.7092	1	0.267
835.958	*5.868*	*14.178*	*10.048*	*0.414*	*0.709*	*3*	*0.000*
834.910	5.8656	14.1742	10.0422	0.4138	0.7085	2	0.736
829.990	5.8540	14.1501	10.0197	0.4137	0.7081	2	1.671
828.770	5.8509	14.1433	10.0153	0.4137	0.7081	2	1.908
824.990	5.8421	14.1221	9.9995	0.4137	0.7081	2	2.640
823.360	5.8380	14.1161	9.9911	0.0414	0.7078	2	2.965
841.648	5.8766	14.2186	10.0728	0.4133	0.7084	1	3.021
819.450	5.8285	14.0943	9.9752	0.4135	0.7077	2	3.796
816.980	5.8225	14.0820	9.9641	0.4135	0.7076	2	4.296
813.430	5.8141	14.0633	9.9484	0.4134	0.7074	2	5.090
810.590	5.8072	14.0478	9.9363	0.4134	0.7073	2	5.707
807.930	5.8007	14.0323	9.9258	0.4134	0.7074	2	6.296
806.350	5.7968	14.0260	9.9175	0.4133	0.7071	2	6.686
804.110	5.7916	14.0081	9.9115	0.4134	0.7076	2	7.231
813.230	5.8094	14.0728	9.9473	0.4128	0.7068	1	9.187
799.264	5.7757	14.0001	9.8845	0.4125	0.7060	1	12.630
785.459	5.7420	13.9275	9.8216	0.4123	0.7052	1	16.335
771.814	5.7083	13.8552	9.7588	0.4120	0.7043	1	20.321

Notes: 1 = this study; 2 = Crichton et al. (1999); and 3 = Finger et al. (1991). Values in italics refer to room conditions for the experiments and to the athermal limit and zero pressure for ab-initio calculations. The last column lists static pressures obtained in this study on the basis of the third-order finite-strain Birch-Murnaghan EOS and values reported by Crichton et al. (1999).

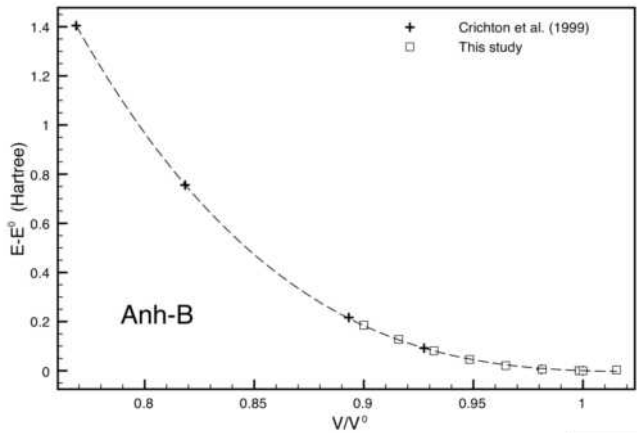

FIGURE 2. Comparison of the calculated potential well of the phase anhydrous B with experimental data.

$$V(0) = \frac{1}{2}\sum_{ij} u_i H_{ij} u_j = \frac{1}{2}\langle u|H|u\rangle \quad (1)$$

where u_i represents a displacement of the ith Cartesian coordinate from its equilibrium value, and H is the Hessian matrix of the second derivatives of $V(\mathbf{x})$, evaluated at equilibrium, with respect to the displacement coordinates

$$H_{ij} = \frac{1}{2}\left[\frac{\partial^2 V(x)}{\partial u_i \partial u_j}\right]_0. \quad (2)$$

In the CRYSTAL code, first derivatives of energy with respect to the atomic positions are calculated analytically (Doll 2001; Doll et al. 2001) for all u_j coordinates, while second derivatives at $\mathbf{u} = 0$ (where all first derivatives are zero) are calculated numerically. We refer to a previous paper (Pascale et al. 2004) for a detailed discussion of the method.

There are 86 atoms in the orthorhombic bypyramidal unit cell so that there are 255 [$(3 \times 86) - 3$] vibrational modes. The irreducible representation of vibrational modes, with a group theoretical treatment of the optical zone-center (Γ point; $\mathbf{k} = 0$), yields

$$\Gamma = 28A_u + 35A_g + 25B_{1g} + 35B_{2g} + 25B_{3g} + 40B_{1u} + 27B_{2u} + 40B_{3u}. \quad (3)$$

In Table 2, we list the vibrational frequencies (ν_i) obtained in this study and their mode-gamma analysis

$$\gamma_i = -\frac{\partial \ln \nu_i}{\partial \ln V} \quad (4)$$

which was carried out by repeating calculations at various expanded state. We are unaware of any experimental data that may be compared with our calculations.

Acoustic modes. At the long-wavelength limit corresponding to the center of the Brillouin zone ($\mathbf{k} \rightarrow 0$) the first three solutions of the dispersion relation

$$\omega = \omega_i(\mathbf{k}) \qquad 1 \le i \le 3n \quad (5)$$

where ω is the angular frequency and n is the number of atoms in the unit cell, vanish (Born and Huang 1954). The first three solutions of the dynamical matrix correspond to homogeneous translation of all atoms in the crystal along the three spatial directions by the effect of an external polarized wave. The propagation of a wave in a continuum may be conveniently described in terms of elongation $\mathbf{u}$ and wavevector $\mathbf{q}$:

$$\mathbf{u} = \mathbf{u}_0 \exp(2\pi i \nu t) \exp(-2\pi i \mathbf{q}\cdot\mathbf{r}) \quad (6)$$

where ν still stands for frequency. The velocity of propagation of the wave is

$$v = \nu/q. \quad (7)$$

Relating the position to the (time-dependent) elongation in vectorial terms:

$$\mathbf{r} = \mathbf{r}_0 + \mathbf{u} \quad (8)$$

where $\mathbf{r}_0$ stands for the equilibrium position defined at each time, t, in terms of elastic constants:

$$c_{ijkl}\frac{\partial u_k}{\partial x_l \partial x_j} = \rho \frac{\partial^2 u_i}{\partial t^2} \quad (9)$$

where ρ is density and c_{ijkl} are the coefficients of the dynamical matrix. Accounting for the elongation expression the above equation was simplified to

$$c_{ijkl} u_k q_l q_l = \rho \nu^2 u_j. \quad (10)$$

The term $\rho\nu^2$ collects the eigenvalues of the dynamical matrix, solved by the Christoffel determinant. The Christoffel determinant has three roots, which depend upon the orientation

TABLE 2. Calculated B3LYP vibrational frequencies for anhydrous B

N	ν (cm^{-1})	Mode	LO-TO	γ_i	N	ν (cm^{-1})	Mode	LO-TO	γ_i	N	ν (cm^{-1})	Mode	LO-TO	γ_i
1	74.4	Acoustic	0.0	–	87	342.4	B_{2u}	−1.1	1.3	173	510.2	B_{1g}	0.0	0.6
2	77.2	Acoustic	0.0	–	88	342.7	A_g	0.0	1.5	174	512.3	B_{3u}	58.8	1.0
3	132.0	Acoustic	0.0	–	89	344.1	B_{1g}	0.0	1.3	175	513.7	B_{2u}	70.9	0.8
4	114.5	B_{3u}	0.1	1.5	90	344.4	B_{1u}	637.3	1.1	176	520.7	A_g	0.0	0.9
5	115.7	A_u	0.0	1.4	91	350.0	B_{2g}	0.0	1.0	177	521.6	B_{1u}	−3.8	0.9
6	120.9	B_{3g}	0.0	1.7	92	350.2	A_u	0.0	2.0	178	525.3	B_{2g}	−1.1	0.9
7	126.1	A_g	0.0	1.7	93	352.0	A_g	−1.8	1.4	179	526.1	B_{3u}	0.0	1.2
8	130.0	A_u	0.0	1.8	94	352.2	B_{1u}	0.0	1.5	180	526.4	B_{3g}	0.0	1.2
9	145.8	B_{1g}	0.0	0.6	95	353.9	B_{3u}	0.7	1.3	181	532.4	A_u	0.0	1.0
10	147.3	B_{1u}	0.1	1.8	96	355.4	B_{1g}	0.0	1.6	182	532.7	B_{2u}	−0.1	1.0
11	164.5	A_g	0.0	1.4	97	355.9	A_g	0.0	2.4	183	535.2	B_{1g}	0.0	0.9
12	165.2	B_{2u}	1.2	2.0	98	360.5	B_{3g}	0.3	2.0	184	536.4	B_{1u}	0.0	1.0
13	172.3	B_{2g}	0.0	0.4	99	360.6	B_{3u}	0.0	1.9	185	538.6	B_{3u}	−0.4	1.1
14	177.8	B_{3U}	0.5	0.8	100	363.4	B_{2u}	0.0	2.0	186	541.4	B_{2g}	0.0	1.2
15	178.8	B_{1g}	0.0	1.2	101	363.5	A_u	19.0	2.0	187	541.7	A_g	0.0	0.5
16	179.1	A_u	0.0	1.1	102	364.6	B_{2g}	0.0	1.8	188	554.5	B_{1u}	0.0	1.1
17	182.4	B_{3g}	0.0	0.4	103	368.6	B_{3g}	0.0	1.7	189	561.7	B_{3u}	−0.2	1.1
18	182.8	B_{1u}	0.1	1.7	104	369.0	B_{2u}	−0.3	1.6	190	562.5	A_g	0.0	1.1
19	195.2	B_{2u}	0.0	1.4	105	369.3	B_{1u}	0.5	1.6	191	570.7	B_{2g}	0.0	0.8
20	195.7	B_{1g}	0.1	2.2	106	371.2	B_{3u}	0.2	1.2	192	571.7	B_{1u}	−16.9	0.8
21	200.0	B_{2u}	0.0	1.1	107	374.5	A_g	0.0	2.0	193	581.9	A_g	0.0	0.6
22	202.9	A_u	0.0	2.1	108	376.7	B_{1g}	0.0	1.9	194	589.7	B_{1u}	−0.3	0.7
23	208.2	B_{1u}	0.5	0.7	109	377.3	A_u	0.0	1.9	195	590.1	B_{2g}	0.0	0.7
24	212.8	B_{3u}	0.7	0.8	110	379.4	B_{2g}	0.0	1.7	196	598.7	A_g	0.9	0.8
25	215.2	B_{3g}	0.0	1.6	111	381.0	B_{1u}	0.0	1.6	197	598.9	B_{3u}	0.0	0.8
26	216.1	B_{1u}	0.4	1.1	112	381.2	A_g	−17.0	1.5	198	603.0	B_{2g}	0.0	0.6
27	217.3	A_u	0.0	0.7	113	381.6	B_{3u}	11.4	1.4	199	604.2	B_{2u}	14.1	0.8
28	218.8	A_g	0.0	0.9	114	385.7	B_{1g}	0.0	1.9	200	606.9	B_{1g}	0.0	0.8
29	221.2	B_{2u}	0.0	1.3	115	389.6	B_{3g}	0.0	1.9	201	608.4	A_u	0.0	0.7
30	224.6	B_{1g}	0.0	1.3	116	393.0	B_{2g}	0.0	1.3	202	612.6	B_{3u}	3.4	0.6
31	224.9	B_{2g}	0.0	1.8	117	396.0	A_u	0.0	1.9	203	613.8	A_g	0.0	0.9
32	227.6	B_{3g}	0.0	1.1	118	396.6	B_{2u}	0.8	1.7	204	614.5	B_{1u}	1.4	0.7
33	231.7	B_{3g}	0.0	1.8	119	399.8	B_{3u}	12.6	1.2	205	615.2	B_{3g}	0.0	0.6
34	235.4	A_u	0.3	0.8	120	403.9	B_{1u}	0.2	1.4	206	619.5	B_{2g}	0.0	0.8
35	238.4	B_{3u}	0.0	2.0	121	405.0	A_u	0.0	2.0	207	620.3	A_u	0.0	0.8
36	238.4	B_{2g}	0.0	1.2	122	405.5	B_{1g}	0.0	1.5	208	622.2	B_{2u}	6.3	0.8
37	240.0	B_{2u}	0.5	1.0	123	406.3	A_g	0.0	1.4	209	624.1	A_g	0.0	0.8
38	242.4	B_{1u}	0.2	1.4	124	408.3	B_{2g}	0.0	1.5	210	626.3	B_{3g}	0.0	1.1
39	243.7	B_{1g}	0.0	1.6	125	409.3	B_{3g}	0.0	1.3	211	631.3	B_{1g}	0.0	0.9
40	245.6	B_{2g}	0.0	1.3	126	413.5	A_g	0.0	1.6	212	634.9	B_{3u}	0.3	0.7
41	248.3	B_{1u}	2.8	0.8	127	419.9	B_{2u}	1.1	2.0	213	638.3	B_{1u}	6.2	0.7
42	255.5	B_{1g}	0.0	0.8	128	420.5	B_{3g}	0.0	1.8	214	649.7	B_{1u}	0.3	0.7
43	255.8	A_u	0.3	1.3	129	420.8	B_{3u}	0.0	1.6	215	653.6	A_g	0.0	0.8
44	257.0	B_{3u}	0.0	1.2	130	420.9	B_{1g}	0.1	1.5	216	656.7	B_{3u}	20.6	0.6
45	259.2	B_{2u}	0.0	1.4	131	421.0	B_{2g}	0.0	1.2	217	665.8	B_{2g}	0.0	0.9
46	260.4	A_g	0.2	2.0	132	423.1	A_g	0.0	1.2	218	674.4	B_{2g}	0.0	0.9
47	262.2	A_g	0.0	1.1	133	426.0	B_{3u}	14.1	1.3	219	683.6	B_{2u}	1.1	0.7
48	266.3	B_{1u}	2.0	0.8	134	429.6	A_u	0.0	1.6	220	684.8	A_u	22.2	0.7
49	267.4	B_{3u}	0.0	1.7	135	429.9	B_{2u}	0.0	1.6	221	685.3	B_{3u}	−90.4	0.6
50	269.5	A_u	0.5	1.5	136	430.5	B_{2g}	9.3	1.7	222	685.6	B_{1u}	0.0	0.7
51	271.0	B_{3u}	0.0	1.6	137	432.0	B_{1u}	0.0	1.6	223	697.2	A_g	0.0	0.5
52	275.2	B_{2g}	0.0	1.2	138	439.3	A_u	0.0	2.0	224	698.1	B_{2g}	0.0	0.5
53	285.6	B_{2g}	0.0	1.5	139	441.3	B_{2g}	0.0	1.4	225	709.0	B_{3u}	58.8	0.8
54	287.3	B_{3g}	0.0	2.5	140	443.2	B_{3g}	−46.4	1.4	226	732.7	B_{1u}	−15.0	0.8
55	288.2	B_{1u}	0.0	1.2	141	443.4	B_{1g}	0.0	1.9	227	793.3	B_{3g}	0.0	1.1
56	290.3	A_g	0.0	2.1	142	443.9	B_{1u}	0.0	1.1	228	794.5	B_{1g}	0.0	1.1
57	290.5	B_{3g}	0.0	1.0	143	443.9	B_{3u}	6.5	1.7	229	798.1	B_{2g}	2.5	1.0
58	292.0	B_{2u}	6.0	1.9	144	446.6	B_{2u}	35.1	1.6	230	798.4	B_{3u}	0.0	1.0
59	293.2	B_{1g}	1.9	1.5	145	447.5	B_{1u}	0.0	1.2	231	798.6	B_{1u}	0.6	1.0
60	295.1	B_{3u}	0.0	2.8	146	447.8	A_g	−2.3	1.5	232	801.3	A_g	0.0	1.0
61	297.6	B_{1g}	0.0	1.9	147	450.0	B_{1u}	−0.5	1.2	233	809.3	B_{2u}	60.2	1.0
62	297.8	B_{1u}	2.2	1.7	148	454.0	B_{3u}	−0.9	1.5	234	811.3	A_u	0.0	1.0
63	298.7	B_{3u}	2.3	1.3	149	454.0	B_{2g}	0.0	1.1	235	829.0	B_{2g}	0.0	0.9
64	299.9	A_u	0.0	1.9	150	454.8	B_{2u}	22.7	1.5	236	835.4	A_g	0.0	0.8
65	303.0	B_{2g}	0.0	1.6	151	455.4	A_g	0.0	1.7	237	848.5	B_{3u}	12.1	0.9
66	306.9	B_{2u}	0.0	1.3	152	455.6	B_{3g}	0.0	1.1	238	855.4	B_{1u}	2.5	0.9
67	307.2	B_{3g}	0.0	1.4	153	463.2	A_g	0.0	1.3	239	855.8	A_g	0.0	1.0
68	307.7	B_{1u}	2.5	1.6	154	463.4	B_{1g}	0.0	1.1	240	866.5	B_{1u}	3.2	0.6
69	311.8	B_{3u}	1.3	1.3	155	466.9	B_{3u}	−0.6	1.3	241	867.8	B_{3u}	9.3	0.7
70	312.8	A_g	0.0	1.5	156	467.2	B_{1u}	0.0	1.3	242	869.4	A_g	0.0	0.6
71	316.5	A_u	0.0	1.7	157	470.8	B_{1g}	0.0	1.4	243	876.2	B_{2g}	0.0	0.9
72	317.6	B_{2u}	0.4	1.9	158	471.6	A_u	0.0	1.3	244	881.7	B_{1u}	4.9	0.8
73	319.2	B_{1g}	0.0	1.1	159	476.0	A_u	−1.4	1.4	245	884.4	B_{3u}	13.9	0.7
74	320.0	B_{3u}	5.0	2.0	160	477.8	B_{3u}	0.0	1.5	246	884.7	B_{2g}	0.0	0.6
75	321.1	B_{2g}	0.0	1.6	161	480.0	B_{2u}	0.0	0.6	247	898.5	A_g	0.0	0.6
76	321.3	B_{3g}	0.0	1.6	162	480.9	B_{3g}	6.2	1.3	248	901.2	B_{1u}	−145.7	0.6

TABLE 2.—*CONTINUED*

N	ν (cm^{-1})	Mode	LO-TO	γ_i	N	ν (cm^{-1})	Mode	LO-TO	γ_i	N	ν (cm^{-1})	Mode	LO-TO	γ_i
77	323.5	B_{1u}	0.0	1.3	163	484.1	A_g	0.0	1.2	249	914.3	B_{1g}	0.0	0.5
78	325.6	B_{3g}	0.0	1.6	164	484.8	B_{2g}	0.0	1.2	250	914.8	A_u	0.0	0.5
79	327.6	B_{3u}	5.8	1.1	165	486.5	B_{1u}	–4.3	1.3	251	917.4	B_{3g}	0.0	0.5
80	328.2	B_{2g}	0.0	1.7	166	488.7	B_{2g}	0.0	0.6	252	918.6	B_{2u}	67.5	0.5
81	332.5	B_{2u}	0.0	1.6	167	493.8	B_{2u}	0.3	1.4	253	955.6	B_{2g}	0.0	0.5
82	333.2	B_{1g}	14.4	2.1	168	497.1	A_u	0.0	1.7	254	968.6	B_{3u}	0.3	0.5
83	335.5	B_{1u}	0.0	1.7	169	497.5	B_{1u}	–4.7	1.4	255	998.7	B_{3u}	51.9	0.9
84	335.7	A_g	4.0	1.7	170	503.7	B_{3g}	0.0	0.6	256	1018.1	A_g	0.0	0.9
85	337.2	A_u	0.0	2.0	171	506.6	B_{3u}	1.7	1.4	257	1033.5	B_{1u}	0.0	0.9
86	340.9	B_{3g}	0.0	1.4	172	509.1	A_u	0.0	0.5	258	1046.5	B_{2g}	0.0	0.8

of the wave vector **q** with respect to the axes of symmetry of the crystal. We transformed the indices of the fourth rank elastic tensor c_{ijkl} to elastic stiffnesses $c_{\alpha\beta}$ (Voigt's notation): $c_{11\rightarrow} c_1$; $c_{22\rightarrow} c_2$; $c_{33\rightarrow} c_3$; $c_{23} + c_{32\rightarrow} c_4$; $c_{13} + c_{31\rightarrow} c_5$; $c_{12} + c_{21\rightarrow} c_6$.

Introducing the Kelvin-Christoffel stiffnesses (Musgrave 1970),

$$\Gamma_{ik} = c_{ijkl} q_i q_l \tag{11}$$

we obtained the Kelvin-Christoffel determinant

$$\begin{vmatrix} \Gamma_{11} - \rho\nu^2 & \Gamma_{12} & \Gamma_{13} \\ \Gamma_{21} & \Gamma_{22} - \rho\nu^2 & \Gamma_{23} \\ \Gamma_{31} & \Gamma_{32} & \Gamma_{33} - \rho\nu^2 \end{vmatrix} = 0. \tag{12}$$

The six independent Kelvin-Christoffel stiffnesses for orthorhombic symmetry are (Cheadle et al. 1991):

$$\Gamma_{11} = q_1^2 c_{11} + q_2^2 c_{66} + q_3^2 c_{55} \tag{13}$$
$$\Gamma_{22} = q_1^2 c_{66} + q_2^2 c_{22} + q_3^2 c_{44} \tag{14}$$
$$\Gamma_{33} = q_1^2 c_{55} + q_2^2 c_{44} + q_3^2 c_{33} \tag{15}$$
$$\Gamma_{23} = q_2 q_3 (c_{23} + c_{44}) \tag{16}$$
$$\Gamma_{31} = q_3 q_1 (c_{31} + c_{55}) \tag{17}$$
$$\Gamma_{12} = q_1 q_2 (c_{12} + c_{66}). \tag{18}$$

Based on the above equations, for a wave vector in the j^{th} direction $q_j = (1,0,0)$ only the diagonal terms are non-zero, and the Kelvin-Christoffel determinant reduces to

$$\begin{vmatrix} \Gamma_{11} - \rho\nu^2 & 0 & 0 \\ 0 & \Gamma_{22} - \rho\nu^2 & 0 \\ 0 & 0 & \Gamma_{33} - \rho\nu^2 \end{vmatrix} = 0. \tag{19}$$

Choosing the eigenvalue $\Gamma_{11} = \rho v^2$ we obtained $v_L = \sqrt{c_{11}/\rho}$ and choosing the other two eigenvalues we got $v_{S1} = \sqrt{c_{66}/\rho}$ and $v_{S2} = \sqrt{c_{55}/\rho}$.

Because the elastic constants are the second derivatives of the energy density with respect to the strain components, that is

$$c_{ij} = \frac{1}{V} \frac{\partial^2 E}{\partial \varepsilon_i \partial \varepsilon_j}\bigg|_0 \tag{20}$$

we were able to evaluate their discrete values by imposing a certain amount of strain ε along the crystallographic direction corresponding to the component of the elastic tensor. Calculations were carried out by using an automatic scheme recently implemented in the CRYSTAL code (Perger et al. 2009). The non-zero elements of the fourth rank strain tensor for Anh-B (Laue class *mmm*) expressed in GPa are listed in Table 3 together with the compliances.

The Voigt and Reuss bounds for bulk modulus (upper = K_V; lower = K_R) and shear modulus (upper = μ_V; lower = μ_R) are given by the following equations, which are valid for any crystal system

$$K_V = \frac{1}{9} \times \left(c' + 2c''\right) = 155.2 \text{ GPa} \tag{21}$$

$$K_R = \left(s' + 2s''\right)^{-1} = 154.7 \text{ GPa} \tag{22}$$

$$\mu_V = \frac{1}{15} \times \left(c' - c'' + 3c'''\right) = 104.5 \text{ GPa} \tag{23}$$

$$\mu_R = 15 \times \left(4s' - 4s'' + 3s'''\right)^{-1} = 103.3 \text{ GPa} \tag{24}$$

where c′ is the sum of the diagonal terms c_{11}, c_{22}, c_{33}; c″ is the sum of the terms c_{12}, c_{13}, c_{23}; c‴ is the sum of the diagonal terms c_{44}, c_{55}, c_{66}; s′ is the sum of the diagonal compliances s_{11}, s_{22}, s_{33}; s″ is the sum of the compliances s_{12}, s_{13}, s_{23}; and s‴ is the sum of the diagonal compliances s_{44}, s_{55}, s_{66}.

The average shear modulus was determined from the Voigt-Reuss-Hill averaging method (VRH; Hill 1952)

$$\overline{\mu}_{VRH} = ½ (\mu_V + \mu_R) = 103.9 \text{ GPa}. \tag{25}$$

Adopting the same averaging procedure for the upper and lower bounds of the bulk modulus one obtains an aggregate bulk modulus $\overline{K}_{VRH} = 154.9$ GPa that is in good agreement with the K_0 value obtained from the BM-EoS based on the various compressional states. This agreement suggests a complete self-consistency of the B3LYP calculation.

Young's modulus, *E*, and Poisson's ratio, ν_P, are respectively,

$$E = \frac{9 K_0 \overline{\mu}_{VRH}}{3K_0 + \overline{\mu}_{VRH}} = 254.8 \text{ GPa} \tag{26}$$

$$\nu_P = \frac{3K_0 - 2\overline{\mu}_{VRH}}{2 \times \left(3K_0 + \overline{\mu}_{VRH}\right)} = 0.226. \tag{27}$$

The average shear and longitudinal wave velocities for the crystalline aggregate are given by

TABLE 3. Calculated B3LYP stiffnesses (c_{ij}) and compliances (s_{ij}) for anhydrous B

Stiffnesses	GPa	Compliances	GPa^{-1}
c_{11}	303.41	s_{11}	372.04×10^{-5}
c_{22}	339.91	s_{22}	322.56×10^{-5}
c_{33}	277.95	s_{33}	413.23×10^{-5}
c_{12}	71.00	s_{12}	-53.99×10^{-5}
c_{13}	88.11	s_{13}	-102.68×10^{-5}
c_{23}	78.52	s_{23}	-74.00×10^{-5}
c_{44}	94.53	s_{44}	1057.86×10^{-5}
c_{55}	103.93	s_{55}	962.18×10^{-5}
c_{66}	96.36	s_{66}	1037.77×10^{-5}

Notes: $D = c_{11}c_{22}c_{33} + 2c_{12}c_{13}c_{23} - (c_{23})^2c_{11} - (c_{12})^2c_{33} - (c_{13})^2c_{22}$ $s_{11} = [c_{22}c_{33} - (c_{23})^2]/D$, $s_{22} = [c_{11}c_{33} - (c_{13})^2]/D$; $s_{33} = [c_{11}c_{22} - (c_{12})^2]/D$; $s_{12} = (c_{13}c_{23} - c_{12}c_{33})/D$; $s_{13} = (c_{12}c_{23} - c_{13}c_{22})/D$; $s_{23} = (c_{13}c_{12} - c_{11}c_{23})/D$; $s_{44} = 1/c_{44}$, $s_{55} = 1/c_{55}$, $s_{66} = 1/c_{66}$.

$$\bar{v}_s = \sqrt{\bar{\mu}_{VRH}/\rho} = 5.570 \left(\frac{km}{s}\right) \quad (28)$$

$$\bar{v}_L = \sqrt{\frac{K_0 + \frac{4}{3} \times \bar{\mu}_{VRH}}{\rho}} = 9.363 \left(\frac{km}{s}\right). \quad (29)$$

To define the acoustic modes, which are to be adopted in the sine-wave dispersion equation of the acoustic branches, we used the non-zero elements of the fourth rank strain tensor calculated by imposing $\mathbf{q} = (1,0,0)$ (Table 3), and thus obtained $\nu_L = 9.519$ km/s; $\nu_{S1} = 5.364$ km/s; $\nu_{S2} = 5.571$ km/s.

The maximum frequency of each acoustic branch was obtained by applying

$$\omega_i = \nu_i \left(\frac{6\pi N_0}{ZV}\right)^{1/3} \quad (30)$$

where the term in brackets (K_{max}) defines the Brillouin zone boundary (i.e., a radius of a sphere with the same volume of the Brillouin zone). Conversion to linear frequencies yields the following results: $\nu_1 = 74.4$ cm^{-1}; $\nu_2 = 77.245$ cm^{-1}; $\nu_3 = 131.986$ cm^{-1}.

Thermochemistry

The quasi-harmonic mode-gamma analysis of the $\alpha_T K_T$ product:

$$\alpha_T K_T = \frac{R}{ZV} \sum_{i=4}^{3n} \gamma_i e^{X_i} \left(\frac{X_i}{e^{X_i} - 1}\right)^2 \quad (31)$$

where X_i is the i^{th} undimensionalized frequency ($X = h\omega/kT$, with h and k, respectively, Planck and Boltzmann constants and ω radial frequency), showed that for Anh-B, it attains at a fairly constant value at high temperature, averaging 0.0050 GPa/K in the T range 1000–3000 K and attaining 0.0051 GPa/K at the $T \to \infty$ limit. From the quasi-harmonic treatment of vibrational frequencies along the guidelines developed in previous investigations (Ottonello et al. 2009a, 2009b; Belmonte et al. 2009) we obtained

$$\frac{\partial K_T}{\partial T} = -189 \left(\frac{bar}{K}\right) \quad (32)$$

(≈ -0.019 GPa/K) and the isobaric thermal expansion of the substance at different temperatures (Fig. 3). The latter data set may be regressed in terms of a polynomial function of temperature:

$$\alpha_T = \alpha_0 T + \alpha_1 + \alpha_2 T^{-1} + \alpha_3 T^{-2} + \alpha_4 T^{-3} \quad (33)$$

with $\alpha_0 = 8.628 \times 10^{-9}$; $\alpha_1 = 2.3086 \times 10^{-5}$; $\alpha_2 = 8.313 \times 10^{-3}$; $\alpha_3 = -4.3445$; $\alpha_4 = 528.465$ ($R^2 = 0.9985$).

In the harmonic approximation the isochoric heat capacity of 1 mole of a substance is

$$C_V = \frac{3R}{Z}\left(\frac{2}{\pi}\right)^3 \sum_{i=1}^{3} \int_0^{X_i} \frac{\left[\arcsin\left(X/X_i\right)\right]^2 X^2 e^X dX}{\left(X_i^2 - X^2\right)^{1/2}\left(e^X - 1\right)^2} + \frac{R}{Z} \sum_{i=4}^{3n} e^{X_i} \left(\frac{X_i}{e^{X_i} - 1}\right)^2 \quad (34)$$

where n is the number of atoms in the unit cell and Z is the number of formula units per unit cell. The first term on the right of Equation 34 is the acoustic contribution at $\mathbf{k}_{max}$ represented in terms of a sine-wave dispersion relation (Kieffer 1979a, 1979b, 1979c). The second term is the contribution of all remaining (optic) modes. The isochoric heat capacity computed at B3LYP level attained, as expected, the Dulong-Petit limit at high temperature.

Using the standard relation between C_P and C_V, i.e.,

$$C_P = C_V + T\alpha_T^2 K_{P,T} V_{P,T} \quad (35)$$

we evaluated C_P (Fig. 4) and translated its T dependency into a Haas-Fisher polynomial (Haas and Fisher 1976) with negligible percent errors (the summation of χ-squared residuals over 28 values is 5.76×10^{-4}).

$$C_P = a + b \times T + c \times T^{-2} + d \times T^2 + e \times T^{-1/2}. \quad (36)$$

Regression coefficients, valid between 298.15 and 3000 K, are as follows: a = 975.27; b = 0.11177; c = $-27.102 \times 10^{+6}$; d = -0.39865×10^{-5}; e = 352.26.

In the absence of configurational disorder, the entropy of 1 mole of a crystalline substance reduces to the following expression:

$$S = \frac{3R}{Z}\left(\frac{2}{\pi}\right)^3 \sum_{i=1}^{3} \int_0^{X_i} \frac{\left[\arcsin\left(X/X_i\right)\right]^2 X dX}{\left(X_i^2 - X^2\right)^{1/2}\left(e^X - 1\right)} - \frac{3R}{Z}\left(\frac{2}{\pi}\right)^3 \sum_{i=1}^{3} \int_0^{X_i} \frac{\left[\arcsin\left(X/X_i\right)\right]^2}{\left(X_i^2 - X^2\right)^{1/2}} \ln\left(1 - e^{-X}\right) dX + \frac{R}{Z} \sum_{i=4}^{3n} \left(\frac{X_i}{e^{X_i} - 1} - \ln\left(1 - e^{-X_i}\right)\right) + \frac{R}{Z} \ln\left(Q_e\right) + \int_0^T V_T K_T \alpha_T^2 dT \quad (37)$$

The first two terms on the right in Equation 37 are the Kieffer model (Kieffer 1979a, 1979b, 1979c) sine-wave dispersion contributions (acoustic modes), the third term is the contribution of the remaining $3n - 3$ (optic) modes, the fourth term is the electronic contribution arising from spin multiplicity (here identically equal to zero) and the last term is the anharmonic contribution to the entropy of the substance. The anharmonic

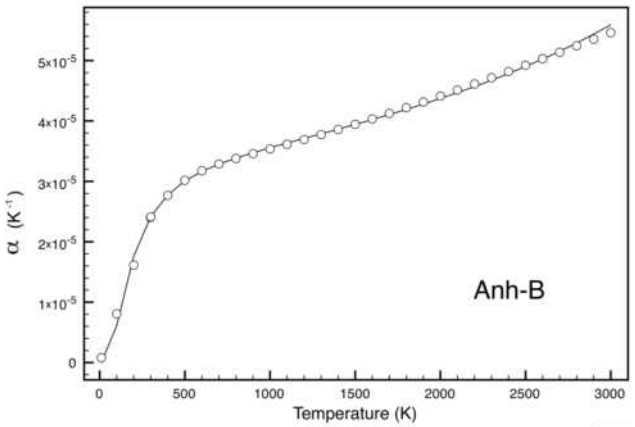

FIGURE 3. Discrete values of the ab-initio thermal expansion of phase anhydrous B (open circles). The solid line is the polynomial regression (33).

term arises formally from the differential increment of isobaric and isochoric heat capacities with T, i.e.,

$$dS_{anh} = \left(C_P - C_V\right)\frac{dT}{T}. \tag{38}$$

However, since α has been derived "quasi-harmonically," the estimate of the last integral in Equation 37 is a quasi-harmonic estimate as well. The bulk entropy, evaluated according to Equation 37, attained a value of 561.2 J/(mol·K) at T = 298.15 K. As we may note in Figure 5, at all temperatures of interest the optic components dominate, and acoustic contributions are subordinate even with respect to anharmonic corrections over most part of the T range of interest.

In the harmonic approximation, the internal energy of a solid is given by

$$U = E_{\text{B3LYP,crystal}} + \frac{3RT}{Z}\left(\frac{2}{\pi}\right)^3 \sum_{i=1}^{3}\int_0^{X_i} \frac{\left[\arcsin\left(X/X_i\right)\right]^2 X dX}{\left(X_i^2 - X^2\right)^{1/2}\left(e^X - 1\right)} + \frac{RT}{Z}\sum_{i=4}^{3n} X_i\left(\frac{1}{2} + \frac{1}{e^{X_i}-1}\right) \tag{39}$$

where the second and third terms on the right constitute the thermal correction to U (ΔU_{T-0}, including the zero-point energy). Knowing U and S, the absolute enthalpy of a substance (H) and the absolute values of its Helmholtz and Gibbs free energies (F and G, respectively) could be obtained by the usual thermodynamic relations ($H = U + PV$; $F = U - TS$; $G = H - TS$). These absolute values should not be confused with the enthalpy and free energy of formation of a substance from elements or oxides that are given in the tabulations of thermodynamic properties. Calculation of the ab-initio enthalpy of formation of a substance from the elements requires the assessment of a thermochemical cycle of the type

$$\bar{H}^0_{f,298.15} = \left(\Delta U_{298.15-0} + P\Delta V_{298.15-0}\right) - D_0 + \sum_{i=1}^{n/Z} n_i H_{f,A_i,0} - \sum_{i=1}^{n/Z} n_i \Delta H_{\text{element}_i,0\to 298.15} \tag{40}$$

where the term within brackets is the thermal correction to the enthalpy at 298.15, $H_{f,A_{i,0}}$ is the enthalpy of formation of the i[th] gaseous atom from the stable element at T = 0 K, P = 1 bar (with the summation extended to the n/Z atoms in the molecule; Table 4), $\Delta H_{\text{element}_i,0\to 298.15}$ is the enthalpy difference between T = 298.15 and T = 0 for the monatomic elements (Table 4) and D_0 is the zero-point dissociation energy of the gaseous molecule into gaseous atoms at 0 K:

$$D_0 = \sum_{i=1}^{n/Z} n_i E_{A_i} - \left(E_{\text{B3LYP,crystal}} + E_{\text{ZPE,crystal}}\right). \tag{41}$$

This energy term corresponds to the sum of the electronic energies of the gaseous atoms at 0 K less the electronic + zero-point energy of the crystal (Table 5).

The estimate of appropriate electronic energies for an isolated gaseous atom is still a matter of debate. One may adopt either the complete theoretical basis set limit or at least add diffuse functions with respect to the basis set adopted in the bulk. A more practical way is to assign to the gaseous atoms electronic energies returning a correct dissociation energy (D_0) of the element at its stable state (i.e., the gaseous diatomic molecule O_2, the cubic hexakisoctahedral crystalline polymorph of Si and the hexagonal close-packed Mg crystal). This requires evaluating the variational structure of the three substances and carrying out their vibrational analysis. The B3LYP energies of gaseous O_2 and crystalline Si, together with their zero-point energies and thermal corrections to U, H, and G were investigated in an

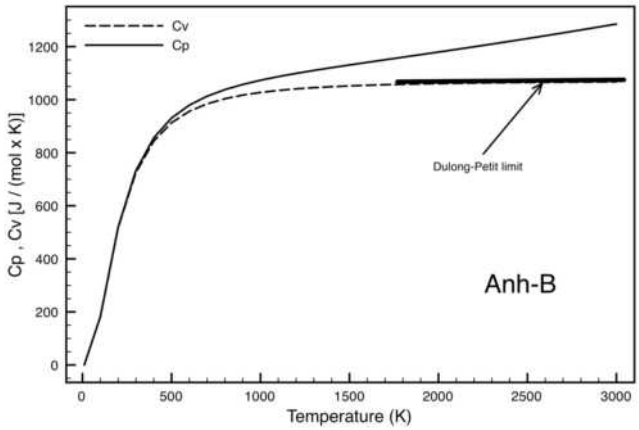

FIGURE 4. Ab-initio isochoric and isobaric heat capacities of the phase anhydrous B. The Dulong-Petit limit is shown for comparison.

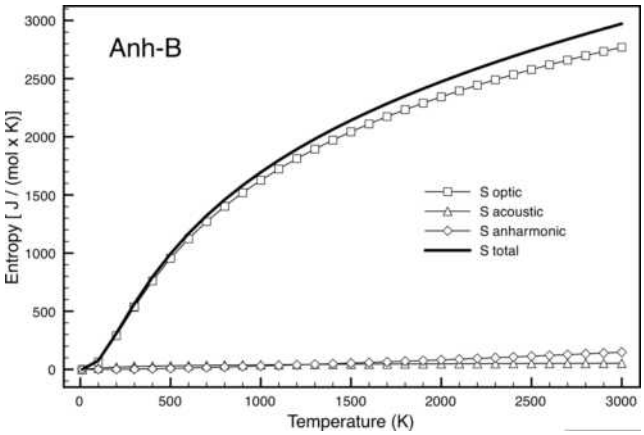

FIGURE 5. Ab-initio entropy terms of the phase anhydrous B.

TABLE 4. Thermochemical reference data for the various atoms of interest in this study

Species	$H_{f,0}$ (kJ/mol)	$\Delta H_{element_i,0\rightarrow298.15}$ (kJ/mol)	$S^{\circ}_{298.15}$ [J/(mol·K)]	E_{A_i}–B3LYP (Hartree)	E_{A_i}*–B3LYP (Hartree)	E_{A_i}† (Hartree)	E_{A_i}‡ (Hartree)
Si	445.668	4.3320	18.820	–280.011087	–	–289.295421	–
O	246.790	4.3415	102.5735	–75.055332	–75.0598419	–75.057906	–
Mg	145.900	4.9980	32.671	–199.766273	–200.044016	–199.910558	–200.013365

Notes: $H_{f,0}$ = enthalpy of formation of the gaseous atom from the stable element at T = 0 K, P = 1 bar (Chase 1998). $\Delta H_{element_i,0\rightarrow298.15}$ is the enthalpy difference between T = 298. 15 K and T = 0 for the monoatomic element (Chase 1998). $S^{\circ}_{298.15}$ is the standard state entropy of the monoatomic element.
* Indicates electronic energies of the gaseous atoms computed respectively with the same basis set of the bulk and with the basis set supplemented by two more diffuse *sp* shells, respectively.
† Indicates the values returning a correct heat content of stable elements at standard state.
‡ Indicates the value returning a correct heat content of forsterite at standard state.

TABLE 5. Ab-initio heat content of the phase Anh-B

Substance	D_0 (kJ/mol)	$H^{\circ}_{f,0}$ (kJ/mol)	$H^{\circ}_{f,298.15}$ (kJ/mol)	$H^{\circ}_{f,0}$ (kJ/mol) / Expt.	$H^{\circ}_{f,298.15}$ (kJ/mol) / Expt.	Ref.
O_{gas}	–	246.8	248.6	246.9 / 246.8	249.4 / 249.2	1,2
Si_{gas}	–	445.7	448.6	445.7 / 451.3	450.0 / 455.6	1,2
Mg_{gas}	–	145.9*	147.0*	145.9 / 146.5	147.1 / 147.7	1,2
O_2 gas	487.4	6.2	0.0	–	0.0	3
Si bulk (cubic)	444.8	0.8	0.0	–	0.0	3
Mg bulk (hexagonal)	142.1*	3.8*	0.0*	–	0.0	3
Anh-B ($Mg_{14}Si_5O_{24}$)	23303.1	–13109.2	–13195.4	–	–	3
Mg_2SiO_4 (forsterite)	3883.7	–2159.1	–2173.0	–	–2173.0	4,5
SiO_2 (stishovite)	1774.1	–834.8	–841.3	–	–861.3	5,6

Notes: 1 = Chase (1998); 2 = Wagman et al. (1982); 3 = this work; 4 = Ottonello et al. (2009a); 5 = Robie and Hemingway (1995); 6 = Ottonello et al. (2009b).
* Calculated with E_{A_i}†. See footnote † in Table 4.

TABLE 6. Thermophysical and thermochemical properties of Anh-B and related parameters

$\bar{v}_L$ (km/s)	9.363	v_L (km/s)	9.519	$V^{\circ}_{298.15}$ (J/bar)	25.870	$S^{\circ}_{298.15}$ [J/(mol·K)]	561.2
$\bar{v}_s$ (km/s)	5.570	v_{S1} (km/s)	5.364	$\rho_{298.15}$ (g.f.w./cc)	3.342	a	975.27
$\bar{v}_\phi$ (km/s)	6.804	v_{S2} (km/s)	5.571	α_0	8.628×10^{-9}	b	0.11177
μ (GPa)	103.9	K_0 (GPa)	155.00	α_1	2.3086×10^{-5}	c	-27.102×10^{6}
E (GPa)	254.8	$(dK/dT)_P$ (GPa/K)	-1.89×10^{-2}	α_2	8.313×10^{-3}	d	-0.39865×10^{-5}
ν_P	0.226	$(dK/dP)_T$	4.14	α_3	–4.3445	e	352.26
				α_4	528.465		

Notes: μ = shear modulus; E = Young's modulus; ν_P = Poisson's ratio; $\rho_{298.15}$ = standard state density; $V^{\circ}_{298.15}$ = standard state volume; $\bar{v}_\phi$ = isotropic average $\bar{v}_\phi = (K_0/\rho)^{1/2}$; $\alpha_{0\rightarrow4}$ = thermal expansion coefficients (Eq. 33). a, b, c, d, e = Haas-Fisher isobaric heat capacity coefficients (Eq. 36).

earlier study (Ottonello et al. 2009b). In evaluating the thermal corrections of silicon, Ottonello et al. (2009b) adopted the acoustic phonons of Brazhkin et al. (2000) and the experimentally determined third law entropy [S° = 18.86 J/(mol·K); Robie and Hemingway 1995]. Because we wanted to evaluate a reaction involving forsterite among the reactants it was considered more appropriate to adopt electronic energies for the isolated atoms that reproduce almost exactly the experimentally observed heat content of this phase. As we may note from the data in Table 4, the electronic energy of gaseous Mg necessary for this purpose is roughly 0.1 Hartree lower than that necessary to reproduce the heat content of metallic Mg.

The thermo-physical and -chemical properties of the Anh-B obtained in this study and thermodynamic functions in the temperature range 298.15–3000 K (P = 1 bar) are summarized in Table 6. The values of thermodynamic functions of the phase at discrete temperatures in the range 298.15–3000 K at 1 bar pressure are listed in Table 7. The thermodynamic functions were calculated as follows: (1) The isochoric heat capacity was obtained by summing up the discrete contributions arising from acoustic and optical harmonic modes at the various T values. (2) The isobaric heat capacity was obtained by adding to the isochoric counterpart the anharmonic contribution represented by the term $T\alpha_T^2K_{P,T}V_{P,T}$ (cf. Eq. 35). (3) The internal vibrational energy of the substance U_{vib} (i.e., the "thermal correction to U" of "quantum chemistry") was again the summation of discrete contributions arising from acoustic and optical modes, but did include the ab-initio static terms (cf. Eq. 39). (4) The vibrational heat content H_{vib} (or "thermal correction to H") was obtained by adding to U_{vib} the P-V product, with the ab-initio volumes. The error in the computed volume has a negligible effect on calculations. (5) The entropy was calculated from the summation of the discrete contributions of acoustic and optical harmonic branches plus the anharmonicity correction (cf. Eq. 37). (6) Thermal expansion and bulk modulus at T and P of interest were obtained from the αK product and its mode-gamma analysis. (7) The vibrational Helmholtz free energy was obtained by subtracting the term TS from U_{vib}; in the same manner one may eventually obtain the thermal correction to G by subtracting TS from H_{vib}. (8) The thermal Gruneisen parameter was evaluated from the relation $\gamma_{thermal} = \alpha_T K_{P,T} V_{P,T}/C_V$. (9) Thermal pressure at T' is the definite integral of the αK_T product from the athermal limit to T' of interest, and was obtained by Gaussian quadrature operated on Equation 31. And, (10) the calorimetric Debye temperature $\Theta_{D,cal}$ was obtained from the bulk isochoric heat capacity (i.e., acoustic + optic contributions) and should not be confused with the "elastic" Debye temperature, which is instead based upon the mean acoustic velocities.

Phase equilibria of Anh-B

It has been shown earlier (Ottonello et al. 2009a, 2009b) that the B3LYP volume of all polymorphs of Mg_2SiO_4 and stishovite are overestimated by ~2.5%. In the case of Anh-B, the molar volume is similarly overestimated by ~2.4 and ~2.8% compared

TABLE 7. Ab-initio B3LYP thermodynamic functions of the phase anhydrous B

T (K)	$K_{T,P}$ (GPa)	$\alpha \times 10^5$ (K^{-1})	$P_{thermal}$ (GPa)	C_V [J/(mol·K)]	C_P [J/(mol·K)]	S [J/(mol·K)]	U_{vib} (kJ/mol)	H_{vib} (kJ/mol)	F_{vib} (kJ/mol)	$\gamma_{thermal}$	$\Theta_{D,cal}$ (K)
298.15	149.365	2.461E-05	0.535	722.8	729.6	561.159	457.4	457.5	290.9	1.280	874.4
300	149.330	2.468E-05	0.541	725.7	732.6	565.685	458.8	458.8	289.9	1.279	875.0
400	147.440	2.842E-05	0.938	843.8	855.9	794.863	537.8	537.8	222.0	1.254	898.9
500	145.550	3.088E-05	1.374	913.2	930.8	994.541	625.9	626.0	133.0	1.246	912.2
600	143.660	3.250E-05	1.831	956.2	979.3	1168.848	719.6	719.6	25.7	1.240	920.1
700	141.770	3.368E-05	2.303	984.4	1013.0	1322.493	816.7	816.7	–97.6	1.236	925.1
800	139.880	3.462E-05	2.785	1003.6	1037.9	1459.432	916.1	916.2	–235.0	1.234	928.3
900	137.990	3.545E-05	3.272	1017.3	1057.3	1582.853	1017.2	1017.2	–384.9	1.234	930.5
1000	136.100	3.621E-05	3.765	1027.3	1073.2	1695.098	1119.5	1119.5	–546.2	1.235	932.0
1100	134.210	3.694E-05	4.260	1034.8	1086.9	1798.057	1222.6	1222.6	–717.7	1.238	933.1
1200	132.320	3.766E-05	4.759	1040.7	1099.1	1893.149	1326.4	1326.4	–898.7	1.242	933.8
1300	130.430	3.837E-05	5.259	1045.3	1110.3	1981.577	1430.7	1430.7	–1088.4	1.247	934.2
1400	128.540	3.908E-05	5.761	1048.9	1120.8	2064.234	1535.4	1535.4	–1286.1	1.252	934.5
1500	126.650	3.980E-05	6.264	1051.9	1130.9	2141.919	1640.5	1640.5	–1491.3	1.257	934.6
1600	124.760	4.052E-05	6.768	1054.4	1140.7	2215.194	1745.8	1745.8	–1703.5	1.263	934.6
1700	122.870	4.125E-05	7.274	1056.4	1150.5	2284.666	1851.3	1851.3	–1922.3	1.269	934.5
1800	120.980	4.198E-05	7.780	1058.1	1160.1	2350.707	1957.0	1957.1	–2147.3	1.275	934.3
1900	119.090	4.273E-05	8.286	1059.6	1169.8	2413.682	2062.9	2063.0	–2378.2	1.281	934.0
2000	117.200	4.348E-05	8.793	1060.9	1179.6	2473.936	2169.0	2169.0	–2614.7	1.287	933.7
2100	115.310	4.424E-05	9.301	1061.9	1189.5	2531.720	2275.1	2275.1	–2856.5	1.293	933.2
2200	113.420	4.500E-05	9.808	1062.9	1199.5	2587.296	2381.3	2381.4	–3103.3	1.298	932.8
2300	111.530	4.577E-05	10.317	1063.7	1209.6	2640.827	2487.7	2487.7	–3355.0	1.303	932.3
2400	109.640	4.654E-05	10.825	1064.4	1219.9	2692.526	2594.1	2594.1	–3611.3	1.308	931.7
2500	107.750	4.732E-05	11.334	1065.1	1230.4	2742.545	2700.6	2700.6	–3872.1	1.312	931.2
2600	105.860	4.810E-05	11.843	1065.6	1241.0	2791.002	2807.1	2807.1	–4137.1	1.316	930.5
2700	103.970	4.889E-05	12.352	1066.1	1251.8	2838.036	2913.7	2913.7	–4406.2	1.320	929.9
2800	102.080	4.968E-05	12.861	1066.6	1262.8	2883.763	3020.3	3020.3	–4679.2	1.323	929.2
2900	100.190	5.048E-05	13.371	1067.0	1273.9	2928.265	3127.0	3127.0	–4956.1	1.325	928.4
3000	98.300	5.128E-05	13.881	1067.3	1285.2	2971.643	3233.7	3233.7	–5236.7	1.327	927.6

to those determined by Finger et al. (1991) and Crichton et al. (1999), respectively, on the basis of single-crystal X-ray data. The fact that the density functional theory overestimates molar volume at the B3LYP level of theory is well known, and there are no known procedures to address this problem. Therefore, we accepted the experimentally determined molar volume at the chosen standard state condition of 1 bar, 298.15 K for all phases involved in the equilibrium A and thus obtained ΔV^o of –1.162 and –1.077 J/bar, using the molar volume of Anh-B determined by Finger et al. (1991) and Crichton et al. (1999), respectively. Combining the thermochemical properties of Anh-B, as determined in this study, with those of forsterite and periclase from the literature [Robie and Hemingway (1995) and Fabrichnaya et al. (2004) for forsterite; Robie and Hemingway (1995), Sinogeikin and Bass (1999), Isaak et al. (1989), Speziale et al. (2001), and Saxena and Shen (1992) for periclase; see Table 8 for details], we obtained the following values for the standard state Gibbs free energy, enthalpy and entropy changes of the reaction A involving pure phases

$$\Delta G° = 81.1 \text{ kJ/mol}, \Delta H^o = 76.0 \text{ kJ/mol},$$
$$\Delta S° = -17.0 \text{ J/(mol·K)}. \quad (42)$$

The equilibrium boundary of reaction A calculated according to the above data and those summarized in Table 8 are compared with the experimental reversals of Ganguly and Frost (2006) in Figure 6. The upper and lower curves correspond to the results of calculation according to the standard state molar volume data of Anh-B by Crichton et al. (1999) and Finger et al. (1991), respectively. The calculated equilibrium boundaries are in good agreement with the experimental data of Ganguly and Frost (2006) when we use the mean value between the two

TABLE 8. Ab-initio B3LYP thermodynamic data for Anh-B and selected literature values for forsterite (Fo) and periclase (Per)

	Anh-B	Fo	Per
V^o_{298} (cc/mol)	251.73–252.58*	43.67†	11.25†
S^o_{298} (J/mol K)	561.2	94.11‡†	26.9†§||
ΔH^o_{f298}(kJ/mol)	–13195.4	–2173.0†	–601.6†§#
K_0 (GPa)	155.0	134.64**††	160.9‡‡
K'_{T_0}	4.14	5.2**,††	4.12§§
$(dK/dT)_P$(bar/K)	–189.0	–248.0**††	–290.0||||
$\alpha_0 \times 10^7$	0.08628	0.139**††	0.0835††
$\alpha_1 \times 10^7$	230.86	201.0**††	364.0††
$\alpha_2 \times 10^3$	8.313	1.627**††	0.85††
α_3	–4.3445	–0.338**††	–0.95††
α_4	528.465	0.0**††	0.0††
$a \times 10^{-2}$	9.7527	1.5779##	0.44728***
$b \times 10^2$	11.177	2.5479##	0.52274***
$c \times 10^{-6}$	–27.102	–3.5973##	–1.1171***
$d \times 10^5$	–0.39865	–0.14651##	–0.011975***
$e \times 10^{-2}$	3.5226	–1.1300##	0.60153***

Notes: The molar volume at T = 298.15 K, P = 1 bar is the experimental datum of Finger et al. (1991). The Haas-Fisher C_P coefficients of Fo have been recalculated in this study by least-squares fitting of the results of Kiseleva et al. (1980), Robie et al. (1982), and Gillet et al. (1991) (T = 298.15 – 1800 K) coupled with the results of the ab-initio investigation of Ottonello et al. (2009a). The C_P coefficients of Per are based of the investigations of Victor and Douglas (1963) and Garvin et al. (1987).

* Finger et al. (1991); Crichton et al. (1999).
† Robie and Hemingway (1995)
‡ Robie et al. (1982).
§ Cox et al. (1989).
|| Chase et al. (1985).
Pankratz and Kelley (1963).
** Fabrichnaya et al. (2004).
†† Saxena and Shen (1992).
‡‡ Sinogeikin and Bass (1999).
§§ Speziale et al. (2001).
|||| Isaak et al. (1989).
Haas-Fisher expansion recalculated in this study on the basis of the investigations of Kiseleva et al. (1980), Robie et al. (1982), and Gillet et al. (1991) and in compliance to the Dulong-Petit limit.
*** Haas-Fisher expansion recalculated in this study on the basis of the investigations of Victor and Douglas (1963) and Garvin et al. (1987) and in compliance to the Dulong-Petit limit.

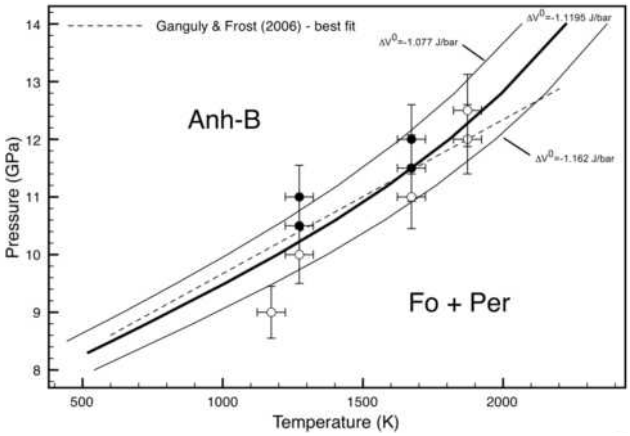

FIGURE 6. The univariant boundary of the equilibrium 5Fo + 4Per ↔ Anh-B calculated from the ab-initio thermodynamic properties of Anh-B, other than molar volume, and literature values of other phases (solid line; see references below), and comparison with the experimental reversals (circles) of Ganguly and Frost (2006) and their best fit curve (dotted line). Filled and open circles = growth of Anh-B at the expense of Fo + Per and the reverse, respectively. $V°$, $S°$, $H°_f$, C_P data are from Robie and Hemingway (1995) for forsterite and periclase; thermal expansion, isothermal bulk moduli K_0, isobaric thermal partial derivative $(\partial K/\partial T)_P$ and isothermal baric partial derivative $(\partial K/\partial P)_T$ are from Fabrichnaya et al. (2004) for forsterite and Sinogeikin and Bass (1999), Isaak et al. (1989), Speziale et al. (2001), and Saxena and Shen (1992) for periclase (see Table 8). The upper and lower curves illustrate the results of calculation using the molar volume of Anh-B determined by Crichton et al. (1999) and Finger et al. (1991), respectively. The bold line refers to results obtained using the mean of the two experimental observations.

experimental observations. There is a gentle curvature of the calculated boundary, with the *P-T* slope increasing with increasing temperature. This curvature, however, could not be resolved by the experimental data of Ganguly and Frost (2006), who fitted their data with a constant *P-T* slope.

In calculating the equilibrium boundary for reaction A, we preferred to use calorimetric data for forsterite and periclase, as much as possible (Robie and Hemingway 1995) since, as noted by Akaogi et al. (2008), the use of internally consistent database assessments to calculate the stability of new phases may yield erroneous results. Small adjustments in the C_P vs. T polynomials of periclase and forsterite were necessary to avoid Dulong-Petit rule violation at high T that one often encounters when extrapolating an original polynomial fit of the C_P vs. T data within a bounded temperature interval. The error introduced is negligible for both phases and inconsequential for the calculation of the phase boundary below 1800 K.

CONCLUDING REMARKS

In this study we have calculated the thermo-chemical and -physical properties of the high-pressure phase Anh-B using hybrid B3LYP density functional theory. The formation of this phase by the reaction between forsterite and periclase (reaction A) may be responsible for the X-discontinuity that has been observed seismically at ~260–330 km depth in a range of mantle conditions. In addition, there could be a splitting of the 410 km seismic discontinuity within a cold subducting slab by the breakdown of wadsleyite and ringwoodite to an isochemical assemblage of Anh-B and stishovite (reaction B).

By combining the thermo-chemical and -physical properties of Anh-B, as determined in this study, with those of forsterite and periclase from the literature, we have calculated the equilibrium boundary for the reaction Fo + Per = Anh-B. The results are in good agreement with the experimental reversal of this boundary by Ganguly and Frost (2006). The molar volume of Anh-B was taken from the literature as density functional theory is known to overestimate the molar volumes of phases.

The agreement between the calculated and experimentally determined equilibrium boundary of reaction A lends confidence to the validity of thermodynamic properties of the Anh-B phase derived in this study, and also testifies to the validity of the method of ab-initio calculations. Similar method was used earlier to calculate the thermodynamic properties of Mg_2SiO_4 polymorphs and stishovite (Ottonello et al. 2007, 2009a, 2009b). After some refinements of the ab-initio thermodynamic properties of these phases, we would calculate the stability field of Anh-B + Stv to evaluate if this assemblage could become stable within the interior of a cold subducting slab.

ACKNOWLEDGMENT

We are indebted to Mauro Prencipe and Mainak Mookherjee for their insightful and constructive remarks.

REFERENCES CITED

Akaogi, M., Kojitani, H., Morita, T., Kawaji, H., and Atake, T. (2008) Low-temperature heat capacities, entropies and high-pressure phase relations of $MgSiO_3$ ilmenite and perovskite. Physics and Chemistry of Minerals, 35, 287–297.

Bagley, B. and Revenaugh, J. (2008) Upper mantle seismic discontinuities of the Pacific. Journal of Geophysical Research, 113, B12301, DOI: 10.1029/2008JB005692.

Belmonte, D., Ottonello, G., and Vetuschi Zuccolini, M. (2009) Ab-initio thermal expansion: the mode gamma analysis in the quasi-harmonic approximation: some examples of application in the Mg-Si-O system. XXXVIII CALPHAD Meeting, Prague, Czech Republic, May 17–22, Abstract, p. 36.

Born, M. and Huang, K. (1954) Dynamical Theory of Crystal Lattices. Oxford University Press, U.K.

Brazhkin, V.V., Lyapin, S.G., Trojan, I.A., Voloshin, R.N., Lyapin, A.G., and Mel'nik N.N. (2000) Anharmonicity of short-wavelength acoustic phonons in silicon at high temperatures. JETP Letters, 72, 195–198.

Chase Jr., M.W. (1998) NIST-JANAF thermochemical tables, Journal of Physical and Chemical Reference Data, Monograph 9. American Chemical Society, Washington, D.C.

Chase Jr., M.W., Davies, C.A., Downey Jr., J.R., Frurip, D.J., McDonald, R.A., and Syverud, A.N. (1985) JANAF Thermochemical Tables 3rd Edition, Part I, Al-Co; Part II, Cr-Zr. Journal of Physical and Chemical Reference Data, 14, Supplement 1, 1856 p.

Cheadle, S.P., Brown, J.R., and Lawton, D.C. (1991) Orthorombic anisotropy: a physical seismic modeling study. Geophysics, 57, 1603–1613.

Cox, J.D., Wagman, D.D., and Medvedev, V.A. (1989) CODATA key values for thermodynamics. Hemisphere, New York.

Crichton, W.A., Ross, N.L., and Gasparik, T. (1999) Equations of state of magnesium silicates anhydrous B and superhydrous B. Physics and Chemistry of Minerals, 26, 570–575.

Cygan, R.T. and Kubicki, J.D., Eds. (2001) Molecular Modeling Theory and Applications in the Geosciences, vol. 42. Reviews in Mineralogy and Geochemistry, Mineralogical Society of America, Chantilly, Virginia.

Doll, K. (2001) Implementation of analytical Hartree-Fock gradients for periodic systems. Computer Physics Communications, 137, 74–88.

Doll, K., Harrison, N.M., and Saunders, V.R. (2001) Analytical Hartree-Fock gradients for periodic systems. International Journal of Quantum Chemistry, 82, 1–13.

Dovesi, R., Saunders, V.R., Roetti, C., Orlando, R., Zicovich-Wilson, C.M., Pascale, F., Civalleri, B., Doll, K., Harrison, N.M., Bush, I.J., D'Arco, P., and Llunell, M. (2006) CRYSTAL06 User's Manual. Università di Torino, Italy.

Fabrichnaya, O.B., Saxena, S.K., Richet, P., and Westrum, E.F. (2004) Thermodynamic Data, Models and Phase Diagrams in Multicomponent Oxide Systems. Springer, New York.

Finger, L.W., Hazen, R.M., and Prewitt, C.T. (1991) Crystal structures of $Mg_{12}Si_4O_{19}(OH)_2$ (phase B) and $Mg_{14}Si_5O_{24}$ (phase AnhB). American Mineralogist, 76, 1–7.

Ganguly, J. and Frost, D.J. (2006) Stability of ahydrous phase B: Experimental studies and implications for phase relations in subducting slab and the X discontinuity in the mantle. Journal of Geophysical Research, 111, B06203.

Garvin, D., Parker, V.B., and White, H.J. (1987) CODATA thermodynamic tables. Selections for some compounds of calcium and related mixtures: A prototype set of tables. Hemisphere, New York.

Gillet, P., Richet, P., Guyot, F., and Fiquet, G. (1991) High-temperature thermodynamic properties of forsterite. Journal of Geophysical Research, 96, 11805–11816.

Haas Jr., J.L. and Fisher, J.L. (1976) Simultaneous evaluation and correlation of thermodynamic data. American Journal of Science, 276, 525–545.

Hill, R.W. (1952) The elastic behaviour of a crystalline aggregate. Proceedings of the Physical Society of London, 65 A, 349–354.

Isaak, D.G., Anderson, O.L., and Goto, T. (1989) Measured elastic moduli of single-crystal MgO up to 1800 K. Physics and Chemistry of Minerals, 16, 704–713.

Kieffer, S.W. (1979a) Thermodynamics and lattice vibrations of minerals: 1. Mineral heat capacities and their relationships to simple lattice vibrational models. Reviews of Geophysics and Space Physics, 17, 1–19.

——— (1979b) Thermodynamics and lattice vibrations of minerals: 2. Vibrational characteristic of silicates. Reviews of Geophysics and Space Physics, 17, 20–34.

——— (1979c) Thermodynamics and lattice vibrations of minerals: 3. Lattice dynamics and an approximation for minerals with application to simple substances and framework silicates. Reviews of Geophysics and Space Physics, 17, 35–59.

Kiseleva, I.A., Ogorodnikova, L.P., Topor, N.D., and Chigareva, O.G. (1980) A thermochemical study of the CaO-MgO-SiO_2 system. Geochemistry International, 16, 122–134.

Musgrave, M.J.P. (1970) Crystal Acoustics. Holdan-Day, Boca Raton, Florida.

Oganov, A.R., Brodholt, J.P., and Price, G.D. (2002) Ab initio theory of phase transitions and thermoelasticity of minerals. In C.M. Gramaccioli, Ed., Energy Modeling in Minerals, 4, p. 83–170. European Notes in Mineralogy, Eötvös University Press, Budapest.

Oganov, A.R., Price, G.D., and Scandolo, S. (2005) Ab initio theory of planetary materials. Zeitschrift für Kristallographie, 220, 531–548.

Ottonello, G., Civalleri, B., Vetuschi Zuccolini, M., and Zicovich-Wilson, C.M. (2007) Ab-initio thermal physics and Cr-isotopic fractionation of $MgCr_2O_4$. American Mineralogist, 92, 98–108.

Ottonello, G., Civalleri, B., Ganguly, J., Vetuschi Zuccolini, M., and Noel, Y. (2009a) Thermophysical properties of the α-β-γ polymorphs of Mg_2SiO_4: A computational study. Physics and Chemistry of Minerals, 36, 87–106.

Ottonello, G., Vetuschi Zuccolini, M., and Civalleri, B. (2009b) Thermo-chemical and thermo-physical properties of stishovite: An *ab-initio* all-electron investigation. CALPHAD, 33, 457–468.

Pankratz, L.B. and Kelley, K.K. (1963) Thermodynamic data for magnesium oxide (periclase). U.S. Bureau of Mines Report of Investigations, 6295, 5 p.

Pascale, F., Zicovich-Wilson, C.M., Lopez-Gejo, F., Civalleri, B., Orlando, R., and Dovesi, R. (2004) The calculation of the vibrational frequencies of crystalline compounds and its implementation in the CRYSTAL code. Journal of Computational Chemistry, 25, 888–897.

Perger, W.F., Criswell, J., Civalleri, B., and Dovesi, R. (2009) Ab-initio calculation of elastic constants of crystalline systems with the CRYSTAL code. Computer Physics Communications, 180, 1753–1759.

Revenaugh, J. and Jordan, T.H. (1991) Mantle layering from ScS reverberations: 3. The upper mantle. Journal of Geophysical Research, 96(B12), 19781–19810.

Robie, R.A. and Hemingway, B.S. (1995) Thermodynamic properties of minerals and related substances at 298.15 K and 1 bar (10^5 Pascals) pressure and at higher temperatures. U.S. Geological Survey Bulletin 2131.

Robie, R.A., Hemingway, B.S., and Takei, H. (1982) Heat capacities and entropies of Mg_2SiO_4, Mn_2SiO_4, and Co_2SiO_4 between 5 and 380 K. American Mineralogist, 67, 470–482.

Saxena, S.K. and Shen, G. (1992) Assessed data on heat capacity, thermal expansion, and compressibility for some oxides and silicates. Journal of Geophysical Research, 97(B13), 19813–19825.

Sinogeikin, S.V. and Bass, J.D. (1999) Single-crystal elasticity of MgO at high pressure. Physical Review B, 59, 14141–14144.

Speziale, S., Zha, C.-S., Duffy, T.S., Hemley, R.J., and Mao, H. (2001) Quasi-hydrostatic compression of magnesium oxide to 52 GPa: Implications for the pressure-volume-temperature equation of state. Journal of Geophysical Research, 106(B1), 515–528.

Stixrude, L., Cohen, R.E., and Hemley, R.J. (1999) Theory of minerals at high pressure. In R.J. Hemley, Ed., Ultrahigh-Pressure Mineralogy: Physics and chemistry of the Earth's deep interior, 37, 639–671. Reviews in Mineralogy, Mineralogical Society of America, Chantilly, Virginia.

Victor, A.C. and Douglas, T.B. (1963) Thermodynamic properties of magnesium oxide and beryllium oxide from 298 to 1200 K. Journal of Research of the National Institute of Standards and Technology, 67A, 325–329.

Wagman, D.D., Evans, W.H., Parker, W.B., Schumm, R.H., Halow, I., Bailey, S.M., Churney, K.L., and Nuttal, R.L. (1982) The NBS tables of chemical thermodynamic properties. Selected values for inorganic and C1 and C2 organic substances in SI units. Journal of Physical and Chemical Reference Data, 11, supplement 2, American Chemical Society and American Institute of Physics for the National Bureau of Standards, New York.

Williams, Q. and Revenaugh, J. (2005) Ancient subduction, mantle eclogite, and the 300 km seismic discontinuity. Geology, 33, 1–4, DOI: 10.1130/20968.1.

Woodland, A.B. (1998) The orthorhombic to high-*P* monoclinic phase transition in Mg-Fe pyroxenes: Can it produce a seismic discontinuity? Geophysical Research Letters, 25, 1241–1244.

MANUSCRIPT RECEIVED AUGUST 6, 2009
MANUSCRIPT ACCEPTED NOVEMBER 1, 2009
MANUSCRIPT HANDLED BY G. DIEGO GATTA